PROCEEDINGS, Fortieth Workshop on Geothermal Reservoir Engineering
Stanford University, Stanford, California, January 26-28, 2015
SGP-TR-204

Enhanced Geothermal Reservoirs with two Fluid Cavities and Unequal Solid and Fluid Temperatures

Rachel M. Gelet[1], Benjamin Loret[2] and Nasser Khalili[3]

1: Université de Nantes, France, 2: Université de Grenoble, France, 3: The University of New South Wales, Sydney, Australia

1: Rachel.Gelet@univ-nantes.fr 2: Benjamin.Loret@grenoble-inp.fr 3: n.khalili@unsw.edu.au

Keywords: local thermal non equilibrium, thermo-hydro-mechanical couplings; thermal stress; double porosity.

ABSTRACT

Thermo-hydro-mechanical (THM) constitutive equations and generalized diffusion and transfer constitutive relations are developed in a comprehensive, coupled and unified framework, assuming a deformable rock formation. Particular attention is laid on both mass and energy exchanges between the cavities which are controlled by the out-of-balances of the chemical potentials and by the out-of-balances of the coldnesses, respectively.

Emphasis is laid a) on the mass exchanges between the pore system and the fracture network, which are endowed each with their own pressure, and mainly; b) on the energy exchanges between the rock, the pore network and the fracture network, which are endowed each with their own temperature.

Thermo-hydro-mechanical (THM) constitutive equations and generalized diffusion and transfer constitutive relations are developed in a comprehensive, coupled and unified framework, assuming a deformable rock formation. Particular attention is laid on both mass and energy exchanges between the cavities which are controlled by the out-of-balances of the chemical potentials and by the out-of-balances of the coldnesses, respectively.

The model is applied to simulate circulation tests using a domestic finite element code. The parameters are calibrated from the thermal outputs of the Fenton Hill and Rosemanowes reservoirs. At variance with a double porosity model with Local Thermal Equilibrium (LTE), the Local thermal Non Equilibrium model (LTNE) displays the characteristic two step time profile that is reported for these two reservoirs. In agreement with field data, fluid loss is observed to be high initially and decreases with time. A sensitivity analysis is performed to determine the influences of the internal length scales, namely fracture spacing and crack aperture, in the complete framework of the dual porosity (2 pressures 2P) and local thermal non equilibrium (3 temperatures 3T) .

The fine description of the effective stress, pore and fracture pressures, and solid, pore and fracture temperatures of the most general format (2P-3T) is essentially unchanged when the model is specialized to (2P-2T) with equal pore and solid temperatures. At variance, the quality of the description is degraded for the (1P-2T) model that omits the permeability contribution of the pores, and for the (1P-1T) standard single porosity LTE model. The progressive transition is quantified during circulation tests at the Fenton Hill HDR.

1 INTRODUCTION

Geothermal energy resources initially tested at Los Alamos National Laboratory, Murphy et al. [1981], continue to attract a significant amount of attention in present-day commercial prototypes, Tenzer [2001]. The development of constitutive models for energy extraction from artificially fractured hot dry rock (HDR) reservoirs requires three main ingredients: (1) a proper thermo-hydro-mechanical coupled model developed from a rational thermodynamic framework; (2) a theory of mixtures for a solid skeleton and one (or several) fluid(s), and (3) local thermal non-equilibrium (LTNE).

The purpose of this work is to contribute to a framework of understanding of the thermo-hydro-mechanical response of fractured media, where, at each geometrical point, the solid skeleton displays two fluid cavities and the temperatures of the solid and fluids are independent. Field observations of pressure buildup and depletion history of reservoirs have demonstrated that standard poro-elasticity may be too crude for a modeling purpose. A more elaborate formulation, such as the dual porosity concept, is needed to provide a reliable description of the effective stress and of the fluid pressures in fractured reservoirs.

As for geothermal energy applications, focus so far has been on partially coupled systems in an effort to implement a network of discrete discontinuities and/or to couple free and forced convection. The closed form solutions by Ghassemi et al. [2005] of the thermally induced stress, in geothermal reservoirs where heat transport is dominated by convection in the fluid phase and by conduction in the solid phase, are worth notice.

Still, the influence of a second porosity, which is not participating to forced convection owing to its low permeability, has been systematically disregarded. Indeed, in spite of their importance in the fields of petroleum engineering, reservoir engineering and geothermal energy extraction, thermo-hydro-mechanical coupling effects in media with double porosity have rarely been investigated. Crucially, the extension of the effective stress concept to media with multiple porosity, and cavities saturated either by liquids or gases, has been an open question for a while. Two propositions remain today: (1) the double effective stress concept, Elsworth and Bai [1992], and (2) the extension of Biot's relationship to dual porosity, Khalili and Valliappan [1996]. The importance of an appropriate definition

of the effective stress is illustrated in the thermo-hydro-mechanical formulations developed for unsaturated porous media, Khalili and Loret [2001].

A key factor in geothermal energy recovery is the difference in the characteristic times between diffusion of heat in the porous blocks and forced convection in the fracture network, a feature that motivates an analysis that allows for local thermal non-equilibrium. In fact, Gelet et al. $[2012]_1$ show that continuum models displaying a single porosity can adequately predict the thermal depletion of hot dry rock reservoirs if LTNE between the solid skeleton and the fluid is accounted for. Still, to the exception of the above work, none of the constitutive models accounting for LTNE in mixtures including a solid and a fluid. Quantifying the inter-phase heat transfer coefficient is essentially an open question in the domain of deformable saturated dual porosity media.

Of crucial importance to the economic viability of enhanced geothermal systems is the knowledge of the induced thermal stresses and of the permeation losses into the porous matrix. Provided that the injection and production wells are appropriately connected, water loss is mainly attributed to the uncontrolled thermal contraction of the rock. Water loss may occur according to three mechanisms: steady state diffusive loss, transient loss into storage and loss due to reservoir growth (propagation of the fracture network). Few studies really address fluid losses into the matrix, permeation being usually imposed by a continuous leak-off into the formation. In contrast, the present approach quantifies the contributions of the two fluid pressures on the thermally induced effective stress and identifies a mechanism of fluid loss.

A fully coupled finite element formulation for a thermo-elastic fractured medium in local thermal non-equilibrium is exposed here. The fractured medium is described as a dual porosity mixture composed of a solid phase and two fluid phases. While Gelet et al. $[2012]_1$ consider a single porosity model with one pore pressure and two temperatures, the dual porosity model displays two pore pressures and three temperatures. The solid phase has a special role as it provides the matrix skeleton and encloses the fluid phases in the porous blocks and the fracture network. The three phase model is embedded within a rational thermodynamic framework. In the finite element implementation, the primary variables are the solid displacement vector, the two pressures of the fluids and the three temperatures of the solid and of the two fluid phases. Comparisons between field data and the simulated response are used to calibrate three parameters of the model so as to match the thermal output, section 4. Particular attention is laid on the magnitude of the specific solid-to-fracture fluid heat transfer coefficient. Once calibrated, the model is used to simulate circulation tests, and the reservoir response is examined in terms of the effective stress and of the permeation of fluid through the porous blocks, section 5. A parametric analysis is performed to explore the response of the model, with special emphasis on the fracture spacing.

2 BALANCE EQUATIONS FOR THE THREE PHASE MIXTURE

Each of the three phases is endowed with its own kinematics, mass and energy content. Accordingly, the thermo-hydro-mechanical response of the mixture requires the partial differential equations in space and time expressing the balances of momentum, the balances of mass and the balances of energy to be satisfied pointwise.

2.1 Basic Definitions

Dual porous media are made of three phases, a solid, a fluid in the pores and a fluid in the fractures. Although the fluids are identical, typically water, the two fluid phases are segregated by their spatial location and are therefore viewed as separate constituents endowed with their own independent pressures and temperatures. In the context of the theory of mixtures, the three phases are viewed as three independent overlapping continua. The solid phase, also referred to as the solid skeleton, has a special role as it serves as a reference. Each phase contains a single constituent, or species, and therefore the two terms could be used interchangeably.

At each point of each phase are defined intrinsic quantities, labeled by subscripts, and apparent or partial quantities, labeled by superscripts. At each point of the fractured porous medium of volume V, the phase k is introduced along with its intrinsic properties of mass M_k and volume V_k. The volumes V_k of the phases sum up to the total volume $V = V_s + V_p + V_f$ of the mixture. The set of all phases is noted by K={ s; p; f } while K^*= {p; f} refers to the set of species which diffuse through the solid skeleton. Each phase k is endowed with a volume fraction n_k, an intrinsic density ρ_k, a partial density ρ^k,

$$n^k = \frac{V_k}{V}, \quad \rho_k = \frac{M_k}{V_k}, \quad \rho^k = \frac{M_k}{V} = n^k \rho_k, \quad k = s, p, f, \tag{1}$$

and an absolute velocity $\mathbf{v}_k$. The volume fractions sum up to one, $n^s + n^p + n^f = 1$. The total mass density of the mixture $\rho = \sum_{k=s,p,f} \rho^k$ is the sum of the apparent contributions. At the reference time t = 0, the total volume V is denoted V_0. The volume content and the mass content of the fluid phase k per unit reference volume of porous medium are denoted by v^k and m^k respectively:

$$v^k = \frac{V_k}{V_0} = n^k \frac{V}{V_0}, \quad m^k = \frac{M_k}{V_0} = \rho_k v^k = \rho^k \frac{V}{V_0} \tag{2}$$

The ratio of the current and reference volumes, V and V_0 respectively, is equal to the determinant of the deformation gradient $\mathbf{F}$, which linearizes to 1 + tr $\boldsymbol{\varepsilon}$ for small strains. The mass flux $\mathbf{m}_k$ and the volume flux $\mathbf{j}_k$ per unit current area of the mixture measure the relative velocity of the fluid phase k with respect to the solid:

$$\mathbf{m}_k = \rho_k \mathbf{j}_k = \rho_k n^k (\mathbf{v}_k - \mathbf{v}_s), \quad k = p, f \tag{3}$$

The solid phase is endowed with its own (infinitesimal) strain tensor $\boldsymbol{\varepsilon} = \frac{1}{2}(\nabla\mathbf{u}+(\nabla\mathbf{u})^{T})$, which is defined from the macroscopic displacement vector $\mathbf{u}$ and which is constitutively decomposed into an elastic contribution $\boldsymbol{\varepsilon}^{el}$ and a thermal contribution $\boldsymbol{\varepsilon}^{\theta}$:

$$\boldsymbol{\varepsilon} = \boldsymbol{\varepsilon}^{el} + \boldsymbol{\varepsilon}^{\theta} \tag{4}$$

The partial stress and pressures of the three phases, $\boldsymbol{\sigma}^{s}$ and pressures p^{k} , which are linked to the intrinsic stress $\boldsymbol{\sigma}_{s}$ and pressures p_{k} of the associated phases through the volume fractions, namely $\boldsymbol{\sigma}^{s} = n^{s}\,\boldsymbol{\sigma}_{s}$, $\boldsymbol{\sigma}^{k} = -n^{k}\,p_{k}\,\mathbf{I}$, k=p,f, sum up to the total stress, namely $\boldsymbol{\sigma} = \boldsymbol{\sigma}^{s} + \boldsymbol{\sigma}^{p} + \boldsymbol{\sigma}^{f}$. The total stress $\boldsymbol{\sigma} = -p\,\mathbf{I} + \mathbf{s}$ and the effective stress $\bar{\boldsymbol{\sigma}} = -\bar{p}\,\mathbf{I} + \mathbf{s}$ may be decomposed into a spherical part and a deviatoric part, by use of the mean stresses $p = -\frac{1}{3}\,\mathrm{tr}\,\boldsymbol{\sigma}$ and $\bar{p} = -\frac{1}{3}\,\mathrm{tr}\,\bar{\boldsymbol{\sigma}}$. The stress components are positive in tension so that the mean stresses p and $\bar{p}$ are counted positive in compression. The elastic strain $\boldsymbol{\varepsilon}^{el} = \mathbf{C}_{*}\bar{\boldsymbol{\sigma}}$ is by definition linked by a one-to-one relationship with the effective stress $\bar{\boldsymbol{\sigma}}$ through the drained compliance tensor C_{*}. In an isotropic context, $\mathrm{tr}\,\boldsymbol{\varepsilon}^{el} = -c_{*}\,\bar{p}$, $\mathbf{e}^{el} = \mathbf{s}\,/2\,\mu_{*}$, in which c_{*} is the drained compressibility of the solid skeleton and μ_{*} its shear modulus. $\mathbf{e}^{el}$ denotes the deviatoric part of the elastic strain $\boldsymbol{\varepsilon}^{el} = \frac{1}{3}\mathrm{tr}\,\boldsymbol{\varepsilon}^{el}\,\mathbf{I} + \mathbf{e}^{el}$. In this isotropic context, the deviatoric parts of the elastic and total strains, $\mathbf{e}^{el}$ and $\mathbf{e}$ respectively, are equal.

Furthermore, the thermodynamical state of each fluid constituent is measured by its pressure p_{k}, its temperature T_{k}, its entropy S_{k} and thermodynamic potentials per unit current mass of the constituent such as the internal energy U_{k}, the free energy E_{k}, the enthalpy H_{k}, and the chemical potential G_{k}, also called free enthalpy:

$$E_{k} = U_{k} - T_{k}S_{k}\,,\ k = s,p,f;\quad H_{k} = U_{k} + \frac{p_{k}}{\rho_{k}},\quad G_{k} = H_{k} - T_{k}S_{k}\,,\ k = p,f \tag{5}$$

Thermodynamic potentials per unit current volume are denoted by a lower letter, e.g. $e^{k} = \rho^{k}\,E_{k}$ for the free energy and $s^{k} = \rho^{k}\,S_{k}$ for the entropy.

2.2 Balances of Momentum, Mass and Energy

A single balance of momentum is required for the mixture as a whole,

$$\mathrm{div}\,\boldsymbol{\sigma} + \rho\mathbf{g} = \mathbf{0} \tag{6}$$

the body force $\rho\mathbf{g}$ due to gravity g and the total mass density ρ being contributed additively by all constituents of the mixture. Since the mass of the solid constituent is constant, a balance of mass is required for the fluid phases only,

$$\mathrm{div}\,\mathbf{j}_{k} + J_{k} = 0,\quad J_{k} = \frac{n^{k}}{\rho_{k}}\frac{d\rho_{k}}{dt} + \frac{1}{V}\frac{dV_{k}}{dt} - \frac{\hat{\rho}^{k}}{\rho_{k}},\quad k = p,f \tag{7}$$

Mass conservation implies the rates of mass change $\hat{\rho}^{k}$ to sum up to zero:

$$\sum_{k=p,f}\hat{\rho}^{k} = 0,\quad \hat{\rho}^{f} = -\hat{\rho}^{p} \tag{8}$$

This study aims to describe the transient period, referred to as local thermal non-equilibrium (LTNE), before the system reaches local thermal equilibrium (LTE). Hence, a balance of energy is required for each phase. Besides terms which are standard for single phases, the energy equations display terms that embody the rate of energy supplied by the phase k to the rest of the mixture $\hat{e}^{k}$, k=s,p,f. The balance of energy for the solid phase accounts for the flux of thermal energy due to conduction $\mathbf{q}_{s}$, the rate of solid entropy and the rate of energy exchange between the solid phase and the other phases:

$$\mathrm{div}\,\mathbf{q}_{s} + Q_{s} = 0,\quad Q_{s} = T_{s}\frac{ds^{s}}{dt} + \hat{e}^{s} \tag{9}$$

The balance of energy for the fluid phase k accounts for the flux of thermal energy due to conduction $\mathbf{q}_{k}$, the rate of fluid entropy, the rates in free energy due to mass transfer, the transfer of energy between the fluid phase k and the other phases, and for forced convection:

$$\mathrm{div}\,\mathbf{q}_{k} + Q_{k} = 0,\quad Q_{k} = T_{k}\frac{ds^{k}}{dt} + \hat{e}^{k} + \hat{\rho}^{k}H_{k} + \mathbf{m}_{k}\cdot\nabla H_{k},\quad k = p,f \tag{10}$$

Energy conservation implies the rates of energy transfer $\hat{e}^{k}$ to sum up to zero:

$$\sum_{k=s,p,f}\hat{e}^{k} = 0,\quad \hat{e}^{s} = -\hat{e}^{p} - \hat{e}^{f} \tag{11}$$

2.3 The Clausius-Duhem Inequality

A single dissipation inequality is required at the mixture level. The dissipation associated with each phase is obtained by inserting the balance of energy into the balance of entropy of each species. The entropy productions of the phases are next summed without multiplying by the phase temperatures. The resulting inequality, referred to as Clausius-Duhem inequality, proves a useful guide to restrict the form of the constitutive couplings. It may be advantageously rewritten in a form that highlights the thermomechanical, transfer and diffusion contributions, $dD = dD_1 + dD_2 + dD_3 \geq 0$, namely

$$\frac{dD_1}{dt} = \sum_{k=s,p,f} \frac{1}{T_k}\left(-\frac{de^k}{dt} + (\boldsymbol{\sigma} - e^k \mathbf{I}) : \nabla \mathbf{v}_s - s^k \frac{dT_k}{dt}\right) + \sum_{k=p,f} \frac{1}{\det \mathbf{F}} \frac{G_k}{T_k} \frac{dm^k}{dt} \geq 0 \tag{12}$$

$$\frac{dD_2}{dt} = -\sum_{k=s,p,f} \hat{e}^k \frac{1}{T_k} - \hat{e}^k_S - \sum_{k=p,f} \left(G_k + \frac{1}{2}(\mathbf{v}_k - \mathbf{v}_s)^2 - \frac{1}{2}\mathbf{v}_s^2\right) \frac{\hat{\rho}^k}{T_k} \geq 0 \tag{13}$$

$$\frac{dD_3}{dt} = \sum_{k=s,p,f} \mathbf{q}_k \cdot \nabla\left(\frac{1}{T_k}\right) - \sum_{k=p,f} \mathbf{j}_k \cdot \frac{\nabla p_k + \rho_k (d^k \mathbf{v}_k / dt - \mathbf{g})}{T_k} \geq 0 \tag{14}$$

which are required to be positive individually, Gelet [2011]. Note that the rate of entropy exchange $\hat{e}^k_s$ between phase k and the other phases of the mixture appears to have no work conjugate variable. The mixture as a whole is assumed to be closed with respect to momentum, equation (6), to mass, equation (8), and to energy, equation (11). Similarly, it is assumed to be closed with respect to entropy, so that the sum of the rates of entropy transfer vanishes $\sum_{k=s,p,f} \hat{e}^k_S = 0$. Therefore the constitutive equations of individual rates of entropy transfer are not needed here. On the other hand, constitutive equations need to be developed for the rates of mass transfer $\hat{\rho}^k$ and the rates of energy transfer $\hat{e}^k$.

A reference configuration is identified, in which the temperatures of the three phases are equal. Departure from this reference state is denoted by the symbol $\Delta(\,)$. The Clausius-Duhem inequality is linearized by (1) neglecting the inertial terms in the transfer contributions dD_2 and in the diffusion contributions dD_3 ; (2) identifying the current and reference configurations so that det **F** may be set to 1. Within an updated Lagrangian analysis, the volume content v^k and the volume fraction n^k are equal at each time, but their rates differ, namely $dv^k = dn^k + n^k \operatorname{tr} \boldsymbol{\varepsilon}$. The same remark applies to the mass content m^k and apparent mass density ρ^k. The thermomechanical contribution to the Clausius-Duhem inequality dD_1 is modified by multiplying by the temperature of the solid constituent T_s:

$$T_s \frac{dD_1}{dt} = -\frac{d\Psi_c}{dt} - \frac{d\boldsymbol{\sigma}}{dt} : \boldsymbol{\varepsilon} - s^s \frac{dT_s}{dt} - \sum_{k=p,f} v^k \frac{dp_k}{dt} \geq 0 \tag{15}$$

$$\frac{dD_2}{dt} = -\sum_{k=s,p,f} \hat{e}^k \frac{1}{T_k} - \sum_{k=p,f} \hat{\rho}^k \frac{G_k}{T_k} \geq 0 \tag{16}$$

$$\frac{dD_3}{dt} = \sum_{k=s,p,f} \mathbf{q}_k \cdot \nabla\left(\frac{1}{T_k}\right) - \sum_{k=p,f} \mathbf{j}_k \cdot \frac{\nabla p_k - \rho_k \mathbf{g}}{T_k} \geq 0 \tag{17}$$

Thermomechanical constitutive assumptions and simplifications are motivated in the next section.

3 CONSTITUTIVE EQUATIONS FOR MASS AND HEAT TRANSFERS

The Clausius-Duhem inequalities (15)–(17) serve as guidelines to develop the constitutive equations, namely (1) The thermomechanical response is constructed in order the thermomechanical dissipation dD_1 to *exactly vanish*. The thermomechanical response of a single fluid k is introduced separately from the thermomechanical elastic equations, Gelet et al. [2012]$_2$; (2) The energy dissipation is due to the transfers of mass and energy between phases, to diffusion of fluids through the solid skeleton and to conduction and convection of heat; (3) The constitutive equations of mass and energy exchanges are expressed in a format that ensures the second dissipation dD_2 to be positive; (4) The constitutive equations of thermal and hydraulic diffusions enforce the third dissipation dD_3 to be positive as well.

3.1 Thermomechanical Elastic Equations

The set of independent variables used so far has tacitly included the strain, the pressures and the temperatures. Alternatively, the total stress might be substituted to the strain as an independent variable. The modification is realized by performing a partial Legendre transform of the elastic potential of the mixture $\Psi(\boldsymbol{\varepsilon}, p_p, p_f, T_s, T_p, T_f)$ that yields the complementary potential $\Psi_c(\boldsymbol{\sigma}, p_p, p_f, T_s, T_p, T_f)$.

At constant total stress and fluid pressures, the sole change of solid temperature leads to a volume change of the solid skeleton, the strain is uniform over the phases, and the volume change of each of the three phases is proportional to its volume fraction. Hence the complementary energy Ψ_c depends on the restricted set of variables $\{\boldsymbol{\sigma}, p_p, p_f, T_s\}$. The vanishing of dD_1 implies that Ψ_c can be used as a thermo-elastic potential that delivers the work conjugate variables $\{\boldsymbol{\epsilon}, v^p, v^f, s^s\}$

$$\text{thermo}-\text{mechanical constitutive equations} \quad \boldsymbol{\varepsilon} = -\frac{\partial \Psi_c}{\partial \boldsymbol{\sigma}}; \quad -v^p = \frac{\partial \Psi_c}{\partial p_p}; \quad -v^f = \frac{\partial \Psi_c}{\partial p_f}; \quad -s^s = \frac{\partial \Psi_c}{\partial T_s} \tag{18}$$

The complementary energy is assumed to be an isotropic quadratic function of the stress, and the sum of a quadratic function and of an affine function of the pressures and solid temperature, Gelet et al. $[2012]_2$. Therefore the deviatoric stress and strain are proportional, $\boldsymbol{\epsilon} = \mathbf{s}/2\,\mu_*$, and the scalar work conjugate variables ($-p$, tr $\boldsymbol{\epsilon}$), (p_p, v^p), (p_f, v^f) and (s^s, T_s) are related by a symmetric and constant matrix. The identification of the constitutive coefficients is best addressed via the equivalent mixed format:

$$\text{linear thermo – mechanical constitutive equations} \quad \begin{bmatrix} p \\ \Delta v^p \\ \Delta v^f \\ \Delta s^s \end{bmatrix} = \begin{bmatrix} -1/c_* & \xi_p & \xi_f & c_T/c_* \\ \xi_p & c_{22} & c_{23} & c_{24} \\ \xi_f & c_{23} & c_{33} & c_{34} \\ c_T/c_* & c_{24} & c_{34} & \rho^s C_s^{(v)}/T_s \end{bmatrix} \begin{bmatrix} \mathrm{tr}\,\boldsymbol{\varepsilon} \\ p_p \\ p_f \\ \Delta T_s \end{bmatrix} \tag{19}$$

The thermomechanical constitutive relations extend the concept of effective stress to dual porosity:

$$\text{effective stress:} \quad \frac{1}{3}\mathrm{tr}\,\boldsymbol{\sigma} + \xi_p\, p_p + \xi_f\, p_f = \frac{1}{c_*}(\mathrm{tr}\,\boldsymbol{\varepsilon} - c_T\,\Delta T_s) \tag{20}$$

The effective stress coefficients $\xi_p = (c_p - c_s)/c_*$ and $\xi_f = 1 - c_p/c_*$ and the coefficients c_{22}, c_{23}, etc. have been identified via a loading decomposition in Khalili and Valliappan [1996] in terms of the drained compressibility of the solid skeleton c_* [1/Pa], the compressibility of the porous blocks c_p, the compressibility of the solid grains c_s, the volumetric thermal expansion coefficient of the solid phase c_T [1/K], and the heat capacity of the solid $C_s^{(v)}$ per unit mass of solid, at constant strain and fluid pressures [J/kg/K]. The constitutive equations for the apparent entropies of the fluids are derived separately from the above relations, Gelet et al. $[2012]_2$.

3.2 Constitutive equations for Mass and Heat Transfers

The constitutive equations of mass and energy exchanges are defined by enforcing the second term of the Clausius-Duhem inequality dD_2 to be positive, equation (16). For that purpose, the rate of mass exchange and the rate of energy exchange are viewed as work-conjugated respectively to the chemical potential scaled by the temperature $-G_k/T_k$ and to the coldness (inverse temperature) $1/T_k$. Due to a lack of in situ measurements and as a first approximation, no coupling is assumed between mass transfer and energy transfer. In other words, the transfer counterparts of the thermo-osmosis and of the isothermal heat transfer in the diffusion constitutive equations developed in section 3.3 are not introduced. The transfers satisfy the closure relations (8) and (11) so that a single mass rate, and two rates of energy exchange associated with the fluids are needed. The inequality (16) yields the restrictions,

$$\begin{aligned} &\text{dissipation due to mass transfer:} \quad -\hat{\rho}^p\left(\frac{G_p}{T_p} - \frac{G_f}{T_f}\right) \geq 0; \\ &\text{dissipation due to heat transfer:} \quad -\hat{e}^p\left(\frac{1}{T_p} - \frac{1}{T_s}\right) - \hat{e}^f\left(\frac{1}{T_f} - \frac{1}{T_s}\right) \geq 0. \end{aligned} \tag{21}$$

The first inequality is satisfied by setting

$$\text{constitutive rate of mass transfer:} \quad \hat{\rho}^p = \eta\,\rho_p^2\,T_{p0}\left(\frac{G_p}{T_p} - \frac{G_f}{T_f}\right) = -\hat{\rho}^f \tag{22}$$

This constitutive equation for mass transfer extends the existing isothermal formulation where the mass transfer is controlled by the difference of pressures between the cavities. The actual leakage parameter $\eta \geq 0$ is defined in section 4.2 ??. The constitutive relations of energy transfer assume the simple linear format,

$$\text{constitutive rates of energy transfer} \quad \begin{bmatrix} \hat{e}^s \\ \hat{e}^p \\ \hat{e}^f \end{bmatrix} = -\begin{bmatrix} -\kappa_{sp} - \kappa_{sf} & \kappa_{sp} & \kappa_{sf} \\ \kappa_{sp} & -\kappa_{sp} - \kappa_{pf} & \kappa_{pf} \\ \kappa_{sf} & \kappa_{pf} & -\kappa_{sf} - \kappa_{pf} \end{bmatrix} \begin{bmatrix} T_s \\ T_p \\ T_f \end{bmatrix} \tag{23}$$

The coefficients κ_{ab}, ab = sp, sf, pf, are volumetric or specific inter-phase heat transfer coefficients [W/m^3/K]. The second inequality $(21)_2$ can be written as a sum of terms $\kappa_{ab}\,(T_a - T_b)^2/(T_a\,T_b)$ over ab = sp, sf, pf, so that the inequality is satisfied if the three specific inter-phase heat transfer coefficients are positive, namely $\kappa_{sp} \geq 0$, $\kappa_{sf} \geq 0$ and $\kappa_{pf} \geq 0$.

3.3 Constitutive Equations for Hydraulic and Thermal Diffusions

The diffusion constitutive equations are similarly defined by enforcing the third term of the Clausius-Duhem inequality $dD_3 \geq 0$. The volume flux $\mathbf{j}_k$, k=p,f, is seen as work-conjugated to the hydraulic gradient $-(\nabla p_k - \rho_k\,\mathbf{g})/T_k$ and the heat flux $\mathbf{q}_k$, k =s,p,f, is conjugated to the thermal gradient $\nabla(1/T_k)$. Since the fluids are segregated by their spatial location, no coupling between the pore fluid diffusion and the fracture fluid diffusion is physically appropriate. For each fluid k, the extended Darcy's law equation describing hydraulic diffusion under combined hydraulic and thermal gradients assumes a coupled format. Similarly, the extended Fourier's law

defining the heat fluxes $\mathbf{q}_k$, k =s,p,f , under combined hydraulic and thermal gradients displays no coupling over phases, but a priori it includes an internal thermo-hydraulic coupling:

$$\begin{aligned} &\text{fluid flux} && \mathbf{j}_k = && -T_k \frac{k_k}{\mu_k}\frac{\nabla p_k - \rho_k g}{T_k} && + n^k T_k^2 \Theta_k \nabla\left(\frac{1}{T_k}\right), && k = p,f; \\ &\text{solid thermal flux} && \mathbf{q}_s = && && n^s T_s^2 \Lambda_s \nabla\left(\frac{1}{T_s}\right); \\ &\text{fluid thermal flux} && \mathbf{q}_k = && -n^k T_k^2 \Phi_k \frac{\nabla p_k - \rho_k g}{T_k} && + n^k T_k^2 \Lambda_k \nabla\left(\frac{1}{T_k}\right), && k = p,f; \end{aligned} \tag{24}$$

Here k_k is the intrinsic permeability [m^2], μ_k is the dynamic viscosity of the fluid [Pa×s] and Θ_k the thermo-osmosis coupling coefficient [m^2/s/K]. The coefficients Φ_k's are called the isothermal heat flow coefficients [m^2/s/K], and the Λ_k's are the thermal conductivities [W/m/K]. Thermo-osmosis and isothermal heat flow mechanisms are likely to be significant in some particular applications such as shale gas extraction and are provided here for completeness. Along Onsager's reciprocity principle, the generalized diffusion matrix linking the vector of fluxes { $\mathbf{j}_p$, $\mathbf{j}_f$,$\mathbf{q}_s$, $\mathbf{q}_p$, $\mathbf{q}_f$ } to the driving gradients {$-\nabla p_p/T_p$., $-\nabla p_f/T_f$., ∇ (1/T_s), ∇ (1/T_p), ∇ (1/T_f)} is assumed symmetric so that the thermo-osmosis coefficients are equal to the isothermal heat flux coefficients: $\Theta_k = \Phi_k$, k=p,f. The Clausius-Duhem inequality (17) is satisfied if the generalized diffusion matrix is positive semi-definite, which is ensured by the inequalities, $\Lambda_k \geq 0,\ k = s,p,f;\ k_k/\mu_k \geq 0,\ k = p,f;\ \Lambda_k\, k_k/\mu_k - n^k T_k\, \Theta_k^2 \geq 0,\ k = p,f.$

4 HDR RESERVOIR ANALYSIS

A finite element formulation is developed for the following primary unknowns: displacement vector **u**, pressure of the pore fluid p_p, pressure of the fracture fluid p_f, temperature of the solid skeleton T_s, temperatures of the pore fluid T_p and of the fracture fluid T_f . Within a generic element e, interpolation in terms of nodal values is realized through the shape functions $\mathbf{N}_u$, $\mathbf{N}_p$, $\mathbf{N}_T$, respectively,

$$\mathbf{u} = \mathbf{N}_u \mathbf{u}^e,\ \ p_p = \mathbf{N}_p \mathbf{p}_p^e,\ \ p_f = \mathbf{N}_p \mathbf{p}_f^e,\ \ T_s = \mathbf{N}_T \mathbf{T}_s^e,\ \ T_p = \mathbf{N}_T \mathbf{T}_p^e,\ \ T_f = \mathbf{N}_T \mathbf{T}_f^e \tag{25}$$

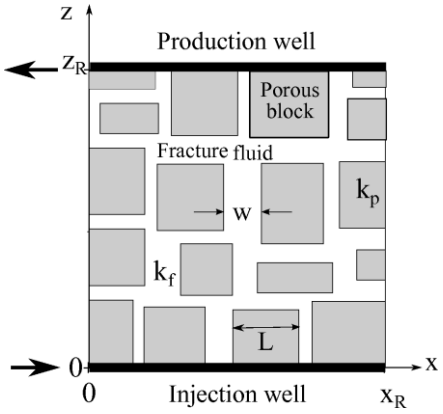

Figure 1: Representation of a generic HDR reservoir. The exact convective flow path is unknown and only the average fracture spacing L and n^f=2w/L the porosity of the fracture network are required to obtain the average fracture aperture w. Here k_p and k_f denote the permeabilities of the porous blocks and of the fracture network, respectively. The simulations assume a plane strain analysis in the x-z plane. Symmetry with respect to z-axis is assumed**.**

4.1 Geometry of the HDR Reservoir, Initial and Boundary Conditions

An artificially fractured reservoir with horizontal injection and production wells is considered, figure 1. The injection and the production wells are located at the bottom and at the top of the reservoir, respectively, and they penetrate the entire horizontal extent of the problem domain x_R. The problem definition requires information on the horizontal and vertical extents of the reservoir x_R and z_R respectively, on the average fracture spacing L, on the average fracture aperture w and on the average permeability of the porous blocks k_p, which provide a second porosity.

Prior to the circulation tests, the reservoir is assumed to be in local thermal equilibrium: the solid and the fluids have identical temperatures $T_0 = T_{s0} = T_{p0} = T_{f0}$. The initial pressures of the fluids $p_{p0} = p_{f0} = \rho_f\, g\, z$ are hydrostatic, proportional to the depth z, with the fluid densities $\rho_p = \rho_f$. The initial stress state is due to the overburden stress $\sigma_{z0} = \sigma_v$ and to the lateral earth stress $\sigma_{x0} = \sigma_H$. Since the fluids are initially in local thermal and hydraulic equilibria, their reference thermodynamic potentials are equal: $S_0 = S_{p0} = S_{f0}$, $G_0 = G_{p0} = G_{f0}$, and $H_0 = H_{p0} = H_{f0}$. Thermal, hydraulic and mechanical boundary conditions (BC) are as follows:

- Thermal BC's: the vertical and upper boundaries are insulated while the temperature is controlled along the injection well;
- Hydraulic BC's: the vertical boundaries are impervious ; the pressure is prescribed along the injection and production wells;
- Mechanical BC's: the motion of the solid is constraint by the symmetry conditions along the axes x and z; the right vertical boundary and the upper horizontal boundary are subject to the geological stress.

The influences of the spatial heterogeneity of the flow path and of the external heat supply on the thermal depletion of the reservoir have been addressed in Gelet [2011]. They are disregarded herein so as to focus on mass and heat exchanges.

4.2 Fracture Spacing Dependence of the Mass and Heat Transfer Coefficients

The fracture spacing L influences three material parameters used in the model, namely (1) the leakage parameter η [1/Pa/s], (2) the specific solid-to-fracture fluid heat transfer coefficient κ_{sf} [W/m^3/K] and (3) the specific pore fluid-to- fracture fluid heat transfer coefficient κ_{pf} [W/m^3/K].

1. The leakage parameter η that controls the flow between the porous blocks and the fracture network draws from Barenblatt et al. [1960]. In this double porosity context, the two cavities symmetrically are not treated symmetrically, and emphasis is put on the permeability of the porous blocks k_p which is lower than the permeability of the fracture network:

$$\text{leakage parameter } \eta = \bar{\alpha}\,\frac{k_p}{\mu_p}, \quad \bar{\alpha} = \frac{4n(n+2)}{L^2} \tag{26}$$

The aperture factor $\bar{\alpha}$ [1/m^2] associated with the lowest permeable phase which has been introduced by Warren and Root [1963] involves the space dimension n (=2 in this plane strain analysis).

2. The specific solid-to-fracture fluid heat transfer coefficient κ_{sf} is defined as the product of the solid-to-fracture fluid specific surface S^s_{sf} [m^2/m^3] with the coefficient of solid-to-fracture fluid heat transfer h_{sf} [W/m^2/K]:

$$\text{specific solid - to - fracture fluid heat transfer coefficient } \kappa_{sf} = h_{sf} \times S^s_{sf} \tag{27}$$

The specific surface $S^s_{sf} = 4n^s/L$ is obtained by considering a porous block square of size L bordered by a fracture fluid of width $w/2 \ll L$. For a given volume fraction $n^f = 2\,w/L$ of the fracture fluid, the average fracture aperture w increases with the fracture spacing L. By assuming that the effect of convection in the fracture fluid phase in the direction orthogonal to the solid-fracture fluid interface is negligible, the coefficient of solid-to-fracture fluid heat transfer h_{sf} may be quantitatively characterized by the sum of the thermal resistances of the two phases in series:

$$S^s_{sf} = \frac{4n^s}{L}, \quad \frac{1}{h_{sf}} = \frac{w}{2n^f\Lambda_f} + \frac{L}{2n^s\Lambda_s}, \quad \kappa_{sf} = h_{sf} \times S^s_{sf} = \frac{8n^s}{L^2}\left(\frac{1}{2\Lambda_f} + \frac{1}{n^s\Lambda_s}\right)^{-1} \tag{28}$$

If $n^s\,\Lambda_s \ll 2\Lambda_f$, the above relation reduces to $\kappa_{sf} = 8(n^s)^2\,\Lambda_s/L^2$ where the two phases are again treated unsymmetrically, à la Warren and Root [1963], and emphasis is put on the most insulating phase.

3. The specific pore fluid-to-fracture fluid heat transfer coefficient κ_{pf} is defined similarly as the product of the pore fluid-to-fracture fluid specific surface S^s_{pf} [m^2/m^3] with the coefficient of pore fluid-to-fracture fluid heat transfer h_{pf} [W/m^2/K], namely for $\Lambda_p = \Lambda_f$, $w \ll L$ and $n^p \ll 1$,

$$S^s_{pf} = \frac{4n^p}{L}, \quad \frac{1}{h_{pf}} = \frac{w}{2n^f\Lambda_f} + \frac{L}{2n^p\Lambda_p} \approx \frac{L}{2n^p\Lambda_p}, \quad \kappa_{pf} = h_{pf} \times S^s_{pf} \approx \frac{8(n^p)^2}{L^2}\Lambda_p \tag{29}$$

Consequently, the three transfer coefficients η, κ_{sf} and κ_{pf} scale with the inverse of the square of the fracture spacing L^{-2}, as illustrated in Table 1 with $k_p = .10^{-20}$ m^2, $n^f = 0.005$, $n^p = 10 \times n^f = 0.05$.

Table 1: Sensitivity of Mass and Heat Coefficients to the Fracture Spacing L.

Coefficient	Unit	L=0.01 m	L=1 m	L=10 m	L=13 m	L=20 m
η	1/Pa/s	3.2×10^{-12}	3.2×10^{-16}	3.2×10^{-18}	1.88×10^{-18}	0.80×10^{-18}
κ_{sf}	W/m^3/K	6.18×10^{4}	6.18	6.18×10^{-2}	3.30×10^{-2}	1.54×10^{-2}
κ_{pf}	W/m^3/K	1.2×10^{2}	1.2×10^{-2}	1.2×10^{-4}	0.71×10^{-4}	0.30×10^{-4}

4.3 Calibration with Field Data

The thermal response obtained from the thermo-hydro-mechanical model may be compared with field data from the literature. Two hot dry rock reservoirs are investigated: (1) Fenton Hill, New Mexico, USA, and (2) Rosemanowes, Cornwall, UK. Initial and boundary conditions and material parameters are documented in Gelet et al. [2012]$_2$. The response in terms of fluid pressures and effective stress for the Fenton Hill HDR reservoir is delayed to section 5. The time profiles of the fracture fluid temperature at the production well are scrutinized alone in figure 2. For a LTNE analysis, the time profile of the temperature depletion is characterized by three stages:

- the first stage represents the abrupt propagation of the injection temperature dominated by convection;
- the second stage characterizes the heat transfer between the fracture fluid phase and the porous blocks;
- the third stage represents the final thermal depletion of the porous medium.

The least well-defined of the material parameters required for a thermo-hydro-mechanical simulation in LTNE are the fracture permeability k_f, the fracture porosity n^f and the solid-to-fracture fluid specific heat transfer coefficient κ_{sf} These coefficients are calibrated so that the numerical response matches the field response based on the following procedure:

- the fracture network permeability k_f is obtained so that the end of the first stage matches the field data;
- the fracture network porosity n^f is adjusted so that the duration of the second stage matches the rest of the response;
- the optimum solid-to-fracture fluid heat transfer coefficient κ_{sf} is obtained so that the temperature magnitude of the second stage best fits the field data.

The three stage history of the outlet temperature shown on figure 2 could not be recovered by a single temperature model (standard thermo-poro-elasticity) which displays a characteristic step-like response (LTE on figure 2).

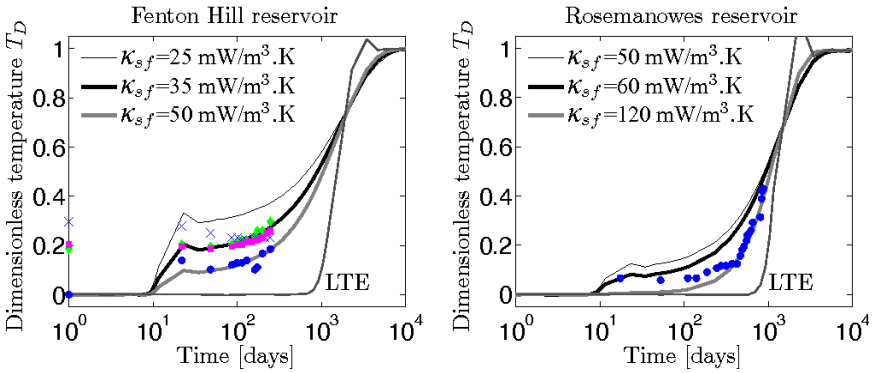

Figure 2. Relative temperature outlet $T_D = (T_0 - T_{prod})/(T_0 - T_{inj})$ versus time in days, with $T_{prod} = T_f(z = z_R)$ the temperature of the fracture fluid at the production well. LTE stands for local thermal equilibrium and is obtained for a large κ_{sf} The late overshooting oscillations for the LTE solution are due to an imperfect damping of the convective contribution, Gelet [2011].
(left) Fenton Hill hot dry rock reservoir with $k_f = 8.0\times10^{-15}$ m^2 and $n^f = 0.005$. Field data pertain to 2703 m (crosses), 2673 m (squares), 2670 m (diamonds) and 2626 m (circles), Zyvoloski et al. [1981]. Optimum $\kappa_{sf} = 33$ mW/m^3/K.
(right) Rosemanowes hot dry rock reservoir with $k_f = 3.2\times10^{-14}$ m^2, $n^f = 0.005$. Field data pertain to circles showing the casing shoe of the production well at 2125 m in true vertical depth, Kolditz and Clauser [1998]. Optimum κ_{sf}=60 to 120 mW/m^3/K.

The specific solid-to-fracture fluid heat transfer coefficients κ_{sf} of the two hot dry rock reservoirs are quite close, which indicates that the order of magnitude is reliable. The comparisons between the field results and the model simulations demonstrate responses in local thermal non-equilibrium, characterized by three stages, which again provides confidence in the LTNE model.

5 THERMO-HYDRO-MECHANICAL RESPONSE

The calibration of the thermo-hydro-mechanical model is now used to perform coupled simulations on the Fenton Hill HDR reservoir. Emphasis is laid on delineating the differences in the response of the geothermal system in terms of temperatures, fluid pressures and effective stress, as inferred by the single and dual porosity models. Special attention is devoted to the fracture spacing L.

For the material parameters associated with the Fenton Hill reservoir, we hypothesize that the dual porosity concept will provide a response in the range between a single porosity model and of a dual porosity model endowed with a low pore permeability. Furthermore, the dual porosity model is endowed with a mass transfer law which allows the permeation of fluid from the fractures toward the pores and conversely. It is expected that large fracture spacings reduce the thermally induced tensile stress and fluid loss: this phenomenon highlights a key feature of sparsely fractured reservoirs with respect to densely fractured reservoirs.

5.1 Dual Porosity Model versus Single Porosity Model

The thermo-hydro-mechanical response of fractured media in a LTNE analysis can be sought with two types of models: (2P-3T) models developed for dual porous media involving two pressures and three temperatures or (1P-2T) models developed for single porous media involving one pressure and two temperatures. Both types are used to predict the thermo-hydro- mechanical behavior of the Fenton Hill HDR reservoir in figures 3 and 4. As a simplification here, the (2P) model considers equal solid and pore fluid temperatures. Still, two sub-options are considered: (i) the pores are connected to each other with a large permeability $k_p = 10^{-18}$ m^2 and (ii) the pores are connected to each other with a low permeability $k_p = 10^{-21}$ m^2 so that both the diffusive flow in the pores and the mass transfer are small.

The dual porosity response with a large pore permeability (and hence large mass transfer) is expected to range between the response of the single porosity model (1P), since no pore pressure counterbalance effect is accounted for in the effective stress, and the dual porosity response with a low pore permeability, since the induced pore pressure will dissipate slowly due to the small mass transfer.

The coupled behavior of fractured media in thermal and hydraulic non-equilibria is governed by the difference in characteristic times between the thermal depletion of the fracture fluid phase and of the solid/pore fluid phases, figure 3. The significant difference in temperature between the fracture fluid and the porous blocks correlates with their highly distinct masses and volumes. Indeed, heat

diffuses by conduction in the porous blocks which are endowed with a large volume fraction $n^s + n^p = 0.995$. On the other hand, the temperature of the fracture fluid propagates by convection and thermal depletion is much faster than in the porous blocks.

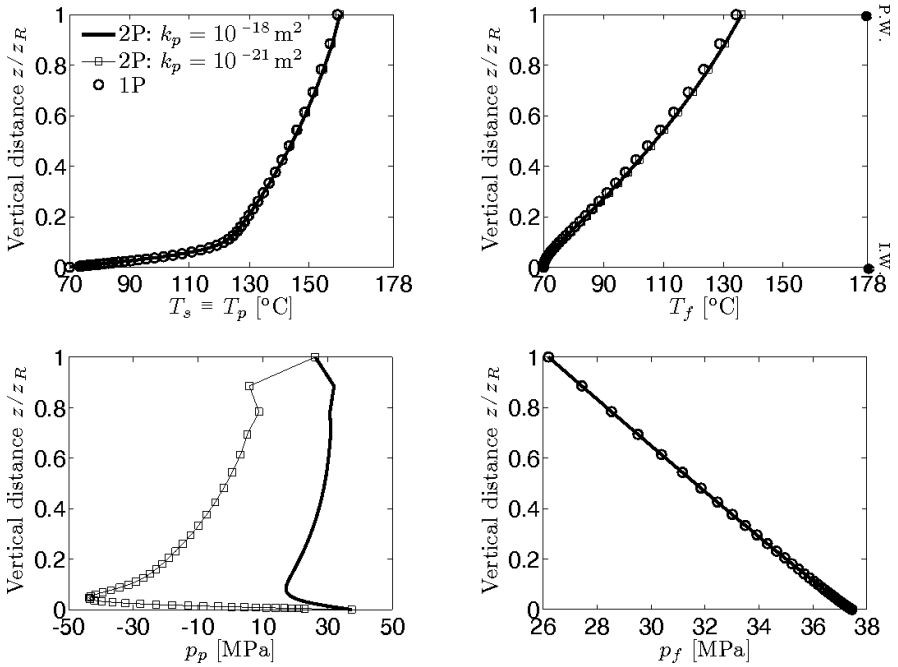

Figure 3: Fenton Hill reservoir, late time (t = 1.9 years) vertical profiles of the (top-left) temperatures of solid and pore fluid, (top-right) temperature of fracture fluid, (bottom-left) pressure of pore fluid, and (bottom-right) pressure of fracture fluid for $k_f = 8.0\times10^{-15}$ m^2, $n^f = 0.005$, $\kappa_{sf} = 33$ mW/m^3/K and L = 13 m. I.W. stands for injection well and P.W. for production well. The responses of the various models match for the temperatures and for the fracture fluid pressure. On the other hand, the pore pressure response of the dual porosity model displays a pressure drop near the injection point. The magnitude of the pressure drop is controlled by the diffusivity ratio $R_p=\sqrt{\alpha_{Hp}/\alpha_{Tp}}$ and is larger for smaller pore permeability ($k_p = 10^{-21}$ m^2).

The solid temperature responses provided by the single porosity model (1P), the dual porosity model (2P) with a large pore permeability ($k_p = 10^{-18}$ m^2) and with a small pore permeability ($k_p = 10^{-21}$ m^2) almost match and are not influenced by the pressure and the strain fields. Hence, the calibration proposed in section 4 remains valid for all models.

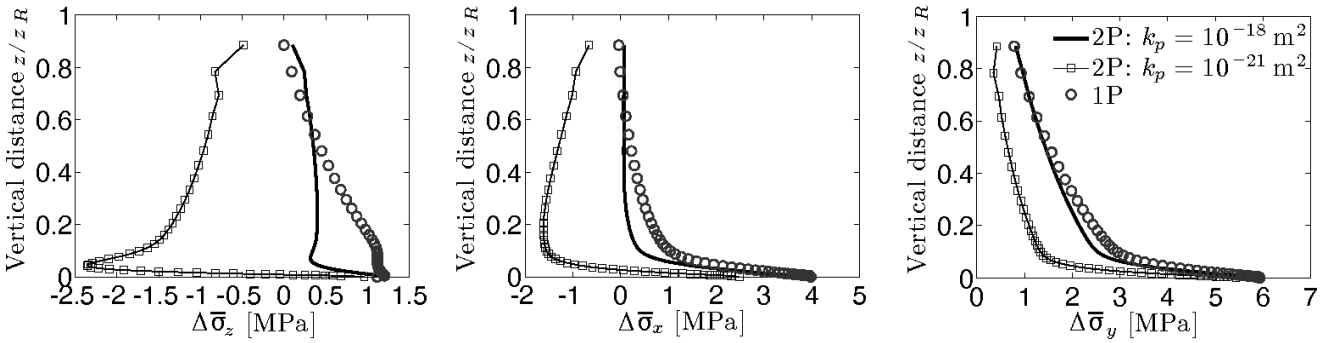

Figure 4: Fenton Hill reservoir, late time (t = 1.9 years) vertical profiles of the changes in (left) vertical effective stress, (middle) lateral effective stress, and (right) out-of-plane effective stress. Tensile stresses are counted positive. Owing to the pore pressure contribution, the stress responses described by the single porosity model (1P) are not equivalent to the responses described by the dual porosity model. The single porosity model predicts a thermally induced tensile stress in the vicinity of the injection well, whereas the dual porosity model predicts a smaller tensile stress ($\Delta\overline{\boldsymbol{\sigma}}_x$ and $\Delta\overline{\boldsymbol{\sigma}}_y$) and an increase of compressive stress ($\Delta\overline{\boldsymbol{\sigma}}_z$.) The pore pressure drop counterbalances the contraction induced by the solid temperature. As expected, close to the injection well $z/z_R < 0.3$, the dual porosity response with $k_p = 10^{-18}$ m^2 is bounded by the dual porosity response with $k_p = 10^{-21}$ m^2 and by the single porosity response which ignores the pore fluid. The sign convention of continuum mechanics is used, and compressive stresses are negative.

As expected from the large fracture permeability $k_f = 8.0\times10^{-15}$ m^2, the response of the fracture fluid pressure varies little from one model to the other as opposed to that of the pore fluid pressure. The dual porosity model displays a decrease in pore pressure induced by the thermal contraction of the solid phase. Indeed, since (1) the pore fluid is embedded into the solid phase which controls fully the

magnitude of the thermal contraction and (2) the coefficient of thermal expansion of the fluid is approximatively 300 times greater than that of the solid phase : the pore pressure decrease is governed by the thermal depletion of the solid phase.

On the other hand, the magnitude of the pore pressure peak is controlled by the hydraulic to thermal diffusivity ratio $R_p=\sqrt{\alpha_{Hp}/\alpha_{Tp}}$. The lower R_p, the larger the pore fluid pressure response. Hence, for the dual porosity model with $k_p = 10^{-21}$ m^2, R_p is small and the pore pressure drop is large compared with the dual porosity model with $k_p = 10^{-18}$ m^2 in which the pore pressure drop dissipates through the connected pores and through mass transfer with the fracture network.

While the thermal depletion of the various phases is the same for all the proposed models, the vertical effective stress is significantly influenced by the pore pressure contribution which tends to damp ($k_p = 10^{-18}$ m^2) or to suppress ($k_p = 10^{-21}$ m^2) the thermally induced tensile stress (1P), figure 4. The effective stress response predicted by the dual porosity model for a large pore permeability is bounded by the single porosity response and by the dual porosity response for a small pore permeability, close to the injection well $z/z_R < 0.3$.

The response of the dual porosity model is fully recovered by the single porosity model for small fracture spacings $L \rightarrow 0$ as presented in the next subsection and on figure 6. Indeed, for very small fracture spacings L, fractured media lose their spatial and time scale separation characteristics, which are the two main hypotheses of the dual porosity concept. Once local thermal and hydraulic equilibria are reached, the dual porosity model is indeed expected to reduce to a single porosity model in LTE with porosity equal to the sum of the fracture and pore porosities and permeability equal to the sum of the fracture and pore permeabilities.

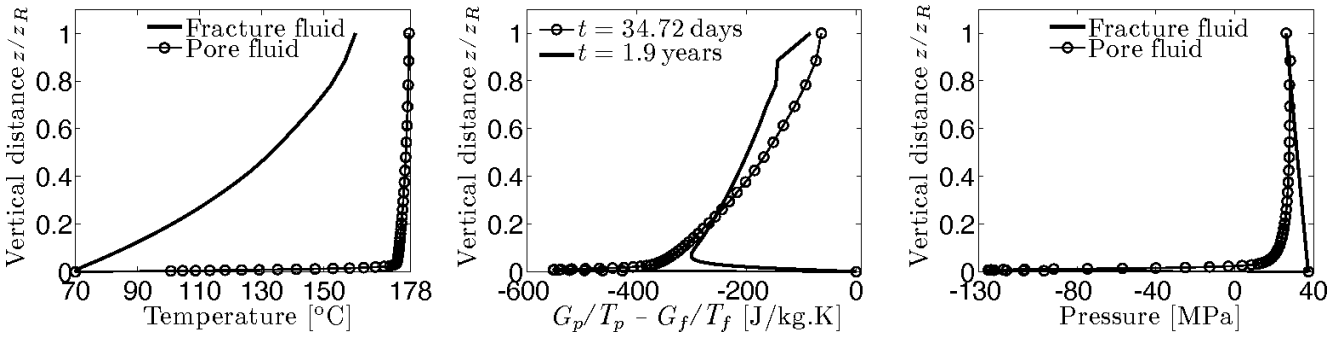

Figure 5: Fenton Hill reservoir, vertical profiles of (left) fluid temperatures at early time (t = 34.72 days), (middle) of jump in scaled chemical potential, and (right) of fluid pressures at early time. At early time, the temperature of the fracture fluid decreases, whereas the temperature of the pore fluid remains high. This large difference associated with a negative difference in scaled chemical potentials $G_p /T_p - G_f /T_f < 0$ induces a large transfer of mass from the fracture network toward the porous blocks, associated with a significant pore pressure drop, while the fracture fluid pressure remains undisturbed as in figure 3. This behavior matches field observations, Murphy et al. [1981].

Moreover, the early mechanism of fluid loss is a consequence of the law of mass transfer induced by the jump in scaled chemical potentials between the two fluids. During the early time t = 34.72 days, the thermal front propagates in the fracture fluid only, while the porous blocks are almost thermally undisturbed as shown in figure 6 for $k_p = 10^{-21}$ m^2 . Consequently, the thermally induced contraction of the pore fluid is small and restricted to the vicinity of the injection well. On the other hand, the temperature difference between the pore fluid and the fracture fluid leads to a large mass transfer from the fractures toward the porous blocks. This large mass transfer is characterized by a large pore pressure drop, to which the thermal contraction contributes partly, and by an increase in compressive effective stress. This model response matches with typical field observations: Murphy et al. [1981] report that the permeation of fluid to the porous blocks is large during the early time and decreases with time.

In summary, the dual porosity model allows a more accurate description of the coupled thermo-hydro-mechanical behavior of fractured reservoirs compared with a single porosity model. In particular, the distinct responses between early time and late time provide information on the permeation mechanism and on the stress path history, which is a key element in view of damage prediction.

5.2 Influence of the Fracture Spacing L

In section 4.2, the mass and heat transfer coefficients have been shown to vary like the inverse of the square of the fracture spacing L. In figures 6, 7 and 8, the influence of the fracture spacing L is considered in the range from 0 to 20 m, so that the lower bound recovers the single porosity response and the upper bound represents a realistic large value, Table 1. For small values of L, LTE between the solid phase and the fluid phases is recovered. Indeed, a small L represents a dense fracture network and reduces the spatial scale and the time scale separation between the porous blocks and the fracture network. Conversely, a large fracture spacing L = 10 m reduces the specific surface area between the solid phase and the fracture fluid phase so that a LTNE model is required.

The fracture spacing L influences greatly the pore pressure response for the reasons explained earlier, whereas the fracture fluid pressure remains undisturbed owing to the large fracture permeability. It is worth noting that hydraulic equilibrium is not recovered unless thermal equilibrium is attained which only takes place for $L \rightarrow 0$ or at large times. This situation is due to the fact that the force driving mass transfer between pores and fractures is non-linear in the form of a difference in scaled chemical potentials, $G_p/T_p - G_f/T_f$.

The change in effective stress results from the deformation and the solid temperature contributions. When both hydraulic and thermal equilibria are reached (L → 0), the effective stress components become more tensile close to the injection area $z/z_R < 0.3$, the final state

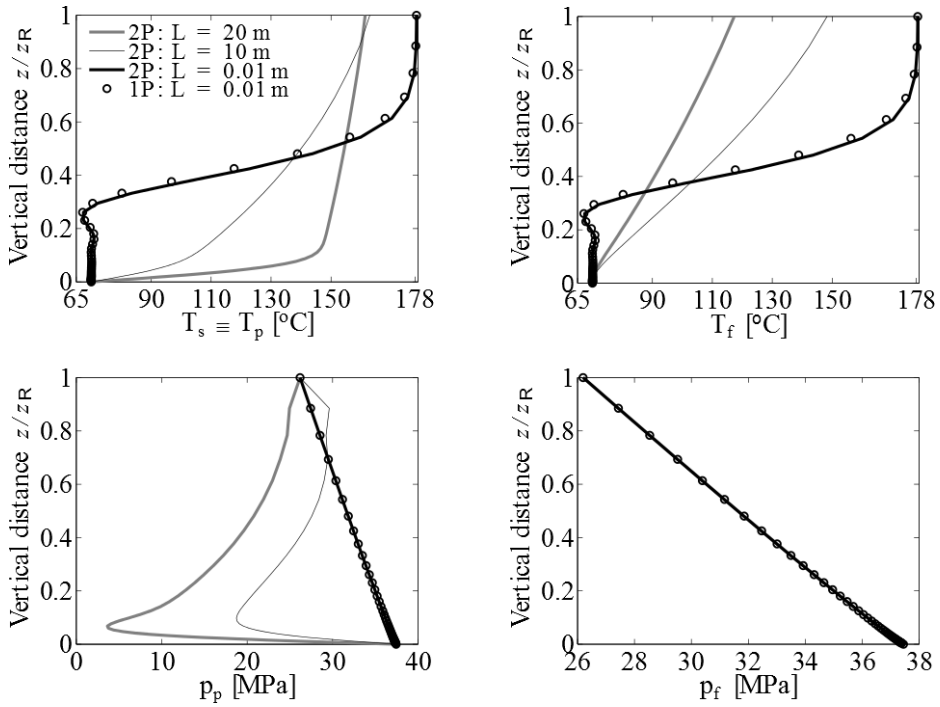

Figure 6: Fenton Hill reservoir, late time (t =1.9 years) vertical profiles of the (top-left) temperatures of solid and pore fluid, (top-right) temperature of fracture fluid, (bottom-left) pressure of pore fluid, and (bottom-right) pressure of fracture fluid for $k_f = 8.0\text{x}10^{-15}$ m^2, $n^f = 0.005$, $k_{sf} = 33$ $mW/m^3/K$. I.W. stands for injection well and P.W. for production well. The responses of the various models match for the temperatures and for the fracture fluid pressure. On the other hand, the pore pressure response of the dual porosity model displays a pressure drop near the injection point. The magnitude of the pressure drop is controlled by the diffusivity ratio R_p and is larger for smaller pore permeability ($k_p = 10^{-21}$ m^2).

being more tensile than the initial state. An increase of fracture spacing L induces simultaneously (1) a departure from thermal equilibrium and thus a slower thermal depletion of the solid phase, and (2) a departure from hydraulic equilibrium and consequently a larger drop in pore pressure. These two contributions entail the change in effective stress by reducing (1) the rate of thermally induced stress and (2) the thermally induced tensile effective stress near the injection point.

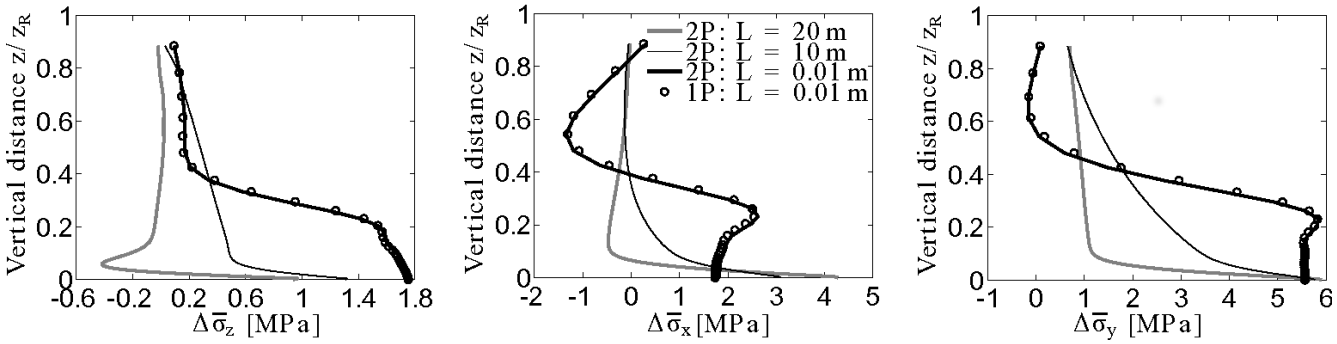

Figure 7: Fenton Hill reservoir, late time (t = 1.9 years). From left to right: vertical profiles of the changes in vertical, lateral and out-of-plane effective stresses for $k_f = 8.0\times10^{-15}$ m^2, $k_p = 10^{-20}$ m^2 and $n^f = 0.005$. For small fracture spacings L → 0, hydraulic and thermal equilibria are reached and the changes in effective stress are tensile close to the injection area $z/z_R < 0.3$. In addition, the single porosity response is well recovered. The dual porosity model reveals that large fracture spacings L reduce the pore pressure and therefore the effective stress $\bar{\boldsymbol{\sigma}} = \boldsymbol{\sigma} + \xi_p\, p_p\, \mathbf{I} + \xi_f\, p_f\, \mathbf{I}$ is more compressive close to the injection well**.**

The thermally induced contraction of the rock may have two adverse effects, a beneficial effect by increasing the aperture of fractures and a negative effect by increasing the aperture of the micro-fractures or pores. The first effect may favor the growth of the reservoir, while the second effect may favor fluid loss. The dual porosity model reveals that large fracture spacings L reduce the thermally induced contraction of the rock in the vicinity of the injection well and thereby the potential for aperture enlargement of the micro-fractures or pores, figure 8. This observation is a signal against fracture clouds composed of many fractures with small spacings and argues in favor of multiple fracture systems with large fracture spacings, Tenzer [2001, Figure 2].

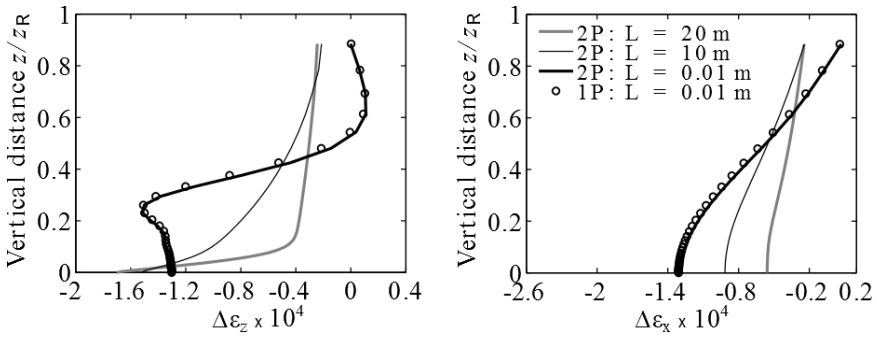

Figure 8: Fenton Hill reservoir, late time (t = 1.9 years) vertical profiles of the changes in (left) vertical strain and (right) lateral strain. For small fracture spacings L → 0, hydraulic and thermal equilibria are reached and negative strains close to the injection area $z/z_R < 0.3$ characterize a sharp thermally induced contraction.

6 CONCLUSIONS

In the current analysis, no attempt has been made to include the spatial heterogeneities of the fracture spacing, fracture porosity, or their directional distribution. Still the issue merits consideration as statistical analyses indicate that the hydraulic permeability in geothermal reservoirs may be controlled by the density of small fractures rather than by large fractures. Furthermore, reservoir growth has been disregarded. Evolution of crack length and aperture due to thermomechanical loadings is the subject of a separate study.

A sensitivity analysis has been carried out to study the influences of the dual porosity model and of the fracture spacing on the phase temperatures, the fluid pressures, and the effective stress. As expected, the dual porosity model provides, close to the injection well, a thermo-hydro-mechanical response which is bounded by the single porosity response and by the dual porosity response endowed with a low pore permeability. The drop in the thermally induced pore pressure is more pronounced when the fracture spacing is large. Hence, large fracture spacings tend to increase the compressive effective stress. In view of potential fluid loss due to the thermally induced rock contraction, this effect advices against densely fractured reservoirs in favor of multiple fracture systems with large fracture spacings.

Accounting only for the fracture fluid and disregarding the pore pressure contribution, the single porosity approach overestimates the thermal contraction of fractured reservoirs. A dual porosity approach delivers information, (1) on fluid permeation in the porous matrix; (2) on the beneficial effect of the pore pressure contribution toward thermally induced stress; (3) on the history of the stress path and (4) on the optimum fracture spacing to reduce fluid loss induced by thermal contraction. Actually, the dual porosity response recovers well the field observations that fluid loss is high at the beginning of the circulation test and decreases with time, e.g. Murphy et al. [1981].

REFERENCES

Barenblatt, G. I, Zheltov, Y. P.and Kochina, I.N.: Basic concepts in the theory of seepage of homogeneous liquids in fissured rocks, *J. Appl. Math. Mech*. (PMM), Engl. Transl., **24**(5), (1960), 1286–1303.

Elsworth, D., and Bai, M.: Flow-deformation response of dual-porosity media, *J. Geotech. Eng.*, (1992), **118**(1), 107–124.

Gelet, R.M.: Thermo–hydro–mechanics of deformable porous media with double porosity and local thermal non–equilibrium, PhD thesis, https://tel.archives-ouvertes.fr/tel-00712459, Université de Grenoble, France (September 2011).

Gelet, R.M., Loret, B. and Khalili, N.: Thermal recovery from a fractured medium in local thermal non-equilibrium, *Int. J. Num. Anal. Methods Geomechanics*, **37**(15), $(2012)_1$, 2471-2501.

Gelet, R.M., Loret, B. and Khalili, N.: A thermo-hydro-mechanical coupled model in local thermal non-equilibrium for fractured HDR reservoir with double porosity, *J. Geophysical Research: Solid Earth,* **117** (B7), $(2012)_2$, 65-76.

Ghassemi, A., Tarasovs, S., and Cheng, A. H.-D.: Integral equation solution of heat extraction-induced thermal stress in enhanced geothermal reservoirs, *Int. J. Num. Anal. Methods Geomechanics*, (2005), **29**, 829–844.

Khalili, N., and Loret, B.: An elasto-plastic model for non-isothermal analysis of flow and deformation in unsaturated porous media formulation, *Int. J. Solids Structures*, (2001), **38**, 8305–8330.

Khalili, N., and Valliappan, S.: Unified theory of flow and deformation in double porous media, *Eur. J. Mech*., (1996), **15**(2), 321–336.

Kolditz, O., and Clauser, C.: Numerical simulation of flow and heat transfer in fractured crystalline rocks: Application to the hot dry rock site in Rosemanowes (U.K.), *Geothermics*, (1998), **27**, 1–23.

Murphy, H. D., Tester, J. W., Grigsby, C. O., and Potter, R. M.: Energy extraction from fractured geothermal reservoirs in low-permeability crystalline rock, *J. Geophysical Research: Solid Earth*, (1981), **86** (B8), 7145–7158.

Tenzer, H.: Development of hot dry rock technology, *Bull. Geo-Heat Center*, **32**, (2001), 14–22.

Warren, J. E., and Root, P. J : The behavior of naturally fractured reservoirs, *Society Petroleum. Eng. J*., (1963), **3**, 245–255.

Zyvoloski, G. A., Aamodt, R. L., and Aguilar, R. G.: Evaluation of the second hot dry rock geothermal energy reservoir: Results of Phase I, Run Segment 5, Tech. Rep. LA-8940-HDR, (1981), 94 pp, Los Alamos Natl. Lab., Los Alamos, N. M., U. S. A.